POLITECNICO DI TORINO
Repository ISTITUZIONALE

Influence of the synthetic procedure on the properties of three Ziegler-Natta catalysts with the same 1,3-diether internal donor

Original
Influence of the synthetic procedure on the properties of three Ziegler-Natta catalysts with the same 1,3-diether internal donor / Milanesi, M.; Piovano, A.; Wada, T.; Zarupski, J.; Chammingkwan, P.; Taniike, T.; Groppo, E.. - In: CATALYSIS TODAY. - ISSN 0920-5861. - 418:(2023). [10.1016/j.cattod.2023.114077]

Availability:
This version is available at: 11583/2985140 since: 2024-01-16T11:45:15Z

Publisher:
Elsevier

Published
DOI:10.1016/j.cattod.2023.114077

Terms of use:

This article is made available under terms and conditions as specified in the corresponding bibliographic description in the repository

Publisher copyright

(Article begins on next page)

20 May 2025

Influence of the synthetic procedure on the properties of three Ziegler-Natta catalysts with the same 1,3-diether internal donor

Matteo Milanesi,[1] Alessandro Piovano,[1,2,3,*] Toru Wada,[2,4] Jelena Zarupski,[1,2] Patchanee Chammingkwan,[2,4] Toshiaki Taniike,[2,4] Elena Groppo[1,2,*]

[1] *Department of Chemistry, INSTM and NIS Centre, University of Torino, Via Giuria 7, 10125 Torino, Italy*

[2] *Dutch Polymer Institute, P.O. Box 902, 5600 AX Eindhoven, The Netherlands*

[3] *GAME Lab, Department of Applied Science and Technology, Polytechnic of Torino, Corso Duca Degli Abruzzi, 24, 10129 Torino, Italy*

[4] *Graduate School of Advanced Science and Technology, Japan Advanced Institute of Science and Technology, 1-1 Asahidai, Nomi, Ishikawa 923-1292, Japan*

Abstract

Being the main responsible for the huge production of polyolefins, heterogeneous Ziegler-Natta catalysts are among the most important catalysts in the chemical industry and they have been optimized over the years since their discovery in 1953 crossing many different generations. Lastly, catalysts of the 5th generation are characterized by the introduction in the pre-catalyst of 1,3-diether compounds as internal electron donors, which are stable in the presence of AlR_3 activators and do not require the further addition of external donors during the following steps of the catalytic process to control the activity and selectivity. In this work, we synthetized and systematically investigated by a multi-technique approach three Ziegler-Natta catalysts characterized by the same 1,3-diether donor, but differing in the synthesis route. We found that the synthetic route influences the $MgCl_2$ particle size, as well as the properties of the Ti species. In particular, the reprecipitation method brings the smallest $MgCl_2$ particles and the most positive Ti^{4+} sites in the pre-catalyst, but also the largest amount of accessible Ti^{3+} sites after TEAl activation. These structural and spectroscopic data correlate pretty well with the kinetic of gas-phase propylene polymerization in very mild conditions.

1. Introduction

Ziegler-Natta (ZN) catalysts are among the most important heterogeneous catalysts employed in chemical industry. They are at the base of the polyolefin production, affording at present almost 80 million tons of polymeric materials per year, with a worldwide economic turnover exceeding 100 billion dollars. Since the discovery of these catalysts in 1953, the expansion of polyolefin market has been closely associated with breakthroughs in the catalysts composition, marking many different generations across seventy years of industrial practice and optimization [1]. Nowadays, the general composition of ZN catalysts for polypropylene production includes $TiCl_4$ species supported on high-surface-area $MgCl_2$ together with some electron donor organic compounds (these three components constitute the so-called pre-catalyst), activated by AlR_3 (typically triethylaluminium, TEAl). The fundamental investigation of ZN catalysts is still a hot topic for both academic and industrial research, since even it would pave the way for a rational optimization of the catalytic process with huge economic profits [2]. The difficulties in defining at a molecular level the structure of the active sites arise from the heterogeneity of the Ti species, the mutual interactions among all the components and the highly flexible nature of the system during the catalytic process [3, 4].

In particular, understanding the effect of different synthesis routes and clarifying the role of electron donors on the catalytic performances are two of the main open questions that still offer challenges for the future development of new and more performant catalysts. Indeed, in ZN catalysis the particle size and the distribution of active sites are determinant for the activity of the catalyst and, in turn, for the properties of the produced polymers. Therefore, along the years many synthetic routes have been explored to get different catalysts able to satisfy different commercial demands for specific applications. These synthetic routes can be divided in two main families, the mechanical and the chemical ones. Mechanical synthesis implies a milling step of $MgCl_2$ support material in the presence of $TiCl_4$ and electron donors, which literally act as capping agents during the formation of the catalyst nanoparticles [5-7]. Among all the chemical routes, one of the most common preparation methods involves the use of $Mg(OEt)_2$ as precursor, which is then converted into $MgCl_2$ by reaction with $TiCl_4$ in organic suspension with the addition of electron donors [8-10]; another common method is the so called solution-reprecipitation, where the $TiCl_4$ is added to a $MgCl_2$ solution up to form a solid compound [11-14].

Each of those synthetic procedures can be further tuned by choosing the proper electron donor. Electrons donors are commonly divided in internal donors (IDs), added during the synthesis of the pre-catalyst, and external donors (EDs), added together with the AlR_3 activator to compensate for the partial loss of ID as a consequence of the reactivity with AlR_3. They contribute to improve the activity, regioselectivity and stereoselectivity of the catalyst. In particular, this work aims at investigating the class of 1,3-diether IDs that marked the 5th generation of ZN catalysts [15]. ZN catalysts with 1,3-diethers as internal donors have unique characteristics, producing polypropylene with narrow molecular weight distribution (MWD), high

hydrogen response and good isotacticity [16-18]. Moreover, in comparison with other electron donors, 1,3-diethers bind at the $MgCl_2$ surface in an unremovable way, competing with $TiCl_4$ at the same adsorption sites [19, 20]. As a consequence, catalysts with 1,3-diether IDs do not require the addition of any ED. According to the literature [19-21], the reason why 1,3-diether donors strongly bind to the $MgCl_2$ surface has to be searched in their very effective coordination mode: indeed, they coordinate preferentially to the (110) $MgCl_2$ surface in a chelate fashion, with both oxygen atoms coordinated to the same Mg^{2+} cation. It is worth noticing that, at least in principle, also the bridging coordination is possible, where the two oxygen atoms bond to two vicinal Mg^{2+} cations, but this configuration was found to be too high in energy from a theoretical point of view [22]. As a consequence of their strong interaction with $MgCl_2$, 1,3-diethers directly influence the stereospecificity of a ZN catalyst. Morini et al. demonstrated that it is possible to tune the stereoselectivity of the 5th generation ZN catalysts by choosing 1,3-diethers with different substituents in position 2: bulkier dialkyl substituents (with long and branched chains) provide the necessary steric hindrance to control the tacticity of the produced polymers, while catalysts containing donors with linear and less bulky substituents display worse performances [23].

In the present work we systematically investigated three different ZN catalysts characterized by the same 1,3-diether donor, but obtained following three different synthetic routes. We characterized the pre-catalysts and the TEAl-activated catalysts by multiple physicochemical techniques and correlated the obtained information with the catalytic performances upon propylene polymerization.

2. Experimental

2.1. Samples preparation and treatments

Three Ziegler-Natta pre-catalysts were synthetized using the same ID, the 2-isopropyl-2-isopentyl-1,3-dimethoxypropane (Figure 1), hereafter referred to as DE, but following different protocols, as follows.

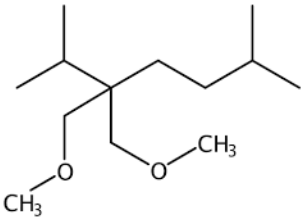

Figure 1. Chemical structure of 2-isopropyl-2-isopentyl-1,3-dimethoxypropane.

ZNC-bm-DE was obtained through a mechanical route. $MgCl_2$ and DE were ball-milled together for 24 hours in a stainless-steel pot sealed under N_2 atmosphere [24]. Afterwards, the so-prepared $MgCl_2$-DE sample was reacted with $TiCl_4$ at 90 °C for 2 hours and finally washed with n-heptane and dried under vacuum.

ZNC-mge-DE was prepared through the chemical conversion of Mg ethoxide precursor by $TiCl_4$. More in details, $Mg(OEt)_2$ was suspended in toluene under stirring. Then, $TiCl_4$ was injected in the suspension at below 0 °C and the mixture was heated up to 60 °C, where DE was added. The temperature was brought to 115 °C and kept for 2 hours. Thereafter, the suspended solid was washed with toluene at 90 °C to remove the reaction by-products, reacted with additional $TiCl_4$, and aged at 115° C for other 2 hours. The resulting solid was finally washed again with toluene and n-heptane at 40 °C and dried under vacuum [25].

ZNC-rep-DE was synthetized through a dissolution-reprecipitation protocol. As first step, $MgCl_2$ was dissolved in a mixture of 2-ethylhexanol (2-EHA) and decane at 120 °C for 2 hours, then the DE donor was added to the solution. Afterwards, the solution was added dropwise to $TiCl_4$ at -15 °C, then slowly heating up the whole system to 90° C. After ageing at that temperature for 2 hours, a solid was obtained, washed with heptane at room temperature, treated with additional $TiCl_4$ again at 90 °C for other 2 hours, filtered, washed again with *n*-heptane, and finally dried in vacuum [26].

The chemical composition of the three pre-catalysts is reported in Table 1.

Table 1. Chemical composition of the pre-catalysts.

Name	Protocol	Ti * [wt%]	Donor ** [wt%]	2-EHA ** [wt%]	OEt ** [wt%]
ZNC-bm-DE	Ball milling	1.1	8.0	n.a.	n.a.
ZNC-mge-DE	$Mg(OEt)_2$	4.3 ± 0.5	16.7 ± 0.8	n.a.	1.35
ZNC-rep-DE	Solution reprecipitation	4.7 ± 0.1	19.1 ± 0.7	0.5 ± 0.1	n.a.

* Determined by a colorimetric method [27].

** Determined with ^{1}H-NMR.

The pre-catalysts were activated at room temperature by impregnating the powders with a diluted solution of triethylaluminium (TEAl) (10 v/v % in hexane), adjusting the amount to get a specific Al:Ti ratio (either 1:1 or 2:1). After impregnation, the activated catalysts were dried by degassing in a high vacuum. Finally, propylene polymerization on the three activated catalysts was carried out in very mild conditions at room temperature, by sending 200 mbar of gas over a known amount of catalyst powder (approximately 0.3 g) inside a quartz reactor of known volume. Propylene pressure was recorded as a function of time: every 5 seconds for the first 30 seconds of reaction, every 10 seconds up to 2 minutes, every 30 seconds up to 5 minutes and every minute until the end of the reaction.

2.2. Characterization methods

To analyse the structure of the $MgCl_2$ support, total scattering experiments were performed at the BL5S6 of Aichi Synchrotron Radiation Center (Aichi, Japan). The details of the measurements and analysis method were described in our previous work [28]. Each catalyst powder was packed in a 0.3 mm diameter Linndemann glass capillary tube and flame-sealed. The monochromated X-ray beam (18.0 KeV) was irradiated to the sample and the scattered X-rays were recorded in the 2Θ = 3–132° range with four 2D detectors. The 2D scattering intensities were converted into 1D diffraction patterns and merged together with the software developed in the beamline. The intensity of an empty capillary was subtracted as the background. In making graphs, the diffraction angle was scaled based on the Cu Kα radiation (8.04 KeV) for direct comparison with literature. The 1D scattering data were converted into reduced atomic pair distribution functions (PDF) with PDFgetX2 [29] with correction for X-ray polarization, Compton scattering, and X-ray atomic scattering factors. In the Fourier transformation, the upper limit of scattering vector *Q* was set as 15.0 $Å^{-1}$ to ensure sufficient statistical accuracy, and the lower limit was set as 1.0 $Å^{-1}$ to eliminate the wavy feature of PDF derived from the nano structures.

IR spectra were measured at a resolution of 2 cm^{-1} with a Bruker Vertex70 FT-IR spectrophotometer, equipped with a MCT detector. The samples were measured in the form of pellets, prepared inside a N_2-filled glove-box and inserted within a quartz cell equipped with two KBr windows, preventing exposure to air. Pristine Ziegler-Natta pre-catalysts were measured diluted in KBr to prevent the saturation of the most intense absorption signals. For CO adsorption experiments, instead, the samples were prepared in the form of undiluted thin self-supporting pellets (surface density of ca. 30 mg/cm^2). The quartz cell was evacuated from nitrogen through a vacuum line and an IR spectrum was collected. After that, CO was introduced in the cell (equilibrium pressure P_{CO} = 100 mbar) and IR spectra were continuously collected at regular time interval for 60 minutes. After that, P_{CO} was decreased stepwise, and the process was monitored by IR spectroscopy. Finally, the IR spectrum of pure DE was recorded in ATR mode with a diamond crystal.

UV−Vis spectra were collected in diffuse reflectance (DR) mode with a Varian Cary5000 spectrophotometer equipped with a reflectance sphere. The powder samples were directly placed inside a bulb-shaped cell made of optical quartz (Suprasil); the filling procedure was accomplished inside the glove-box to avoid contamination by air. The spectra have been collected in the reflectance mode and then converted in Kubelka−Munk function.

3. Results and discussion

3.1. Structural and spectroscopic investigation of the ZN pre-catalysts

3.1.1. Structural characterization

The XRD patterns of the pre-catalyst samples are reported in Figure 2. For reference, the pattern of α-$MgCl_2$ is shown together with the assignment of corresponding Bragg reflection planes. It has been reported that the extent of activation of $MgCl_2$ support is related to three structural disorders [28]. Namely, the thickness of the $MgCl_2$ lamellar crystal (L_c), its dimension in the lateral direction (L_a, L_b), and the stacking disorder among Cl-Mg-Cl layers (P_c). P_c is the probability that the Cl atoms are arranged as cubic closest packing (ABCA), with 100% being α-$MgCl_2$ and 25% being completely random stacking. Each disorder can be associated with a specific peak in α-$MgCl_2$. That is, L_c primarily broadens the peak of (003) planes, L_a and L_b the peaks of (110) planes, and P_c the peaks of (012) and (104) planes [28].

For ZNC-bm-DE, where $MgCl_2$ was mechanically activated in the presence of DE, the peaks representative of the (003), (012), (104), and (110) planes were all broader than for α-$MgCl_2$, indicating that the structure of the $MgCl_2$ support was disordered. The other two catalysts prepared by chemical routes showed this trend more strongly. That is, the representative diffraction peaks became even broader, while the lower intensity peaks ((101), (107), and (018)), which were visible in the pattern of ZNC-bm-DE, disappeared completely. Hence, the chemical routes yielded even more disordered $MgCl_2$ supports than the mechanical activation. On the other hand, these two catalysts were almost qualitatively indistinguishable in terms of diffraction patterns.

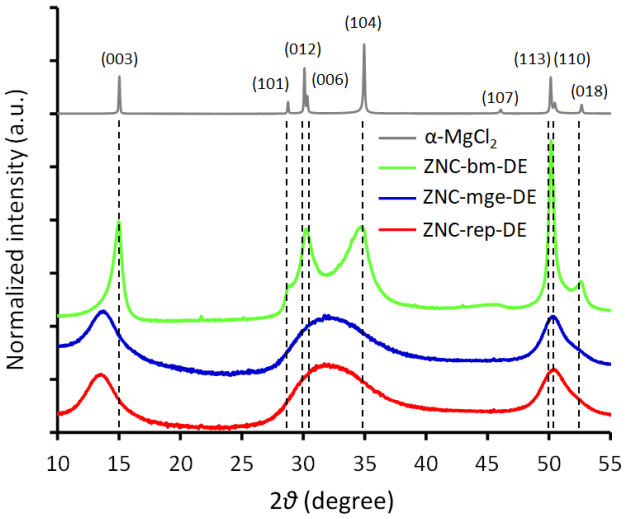

Figure 2. PXRD patterns of ZNC-bm-DE (green), ZNC-mge-DE (blue), and ZNC-rep-DE (red). All the patterns were extracted from the total scattering data and vertically translated for clarity. The intensity was normalized with the total intensity within the shown 2Θ range. The diffraction pattern of α-$MgCl_2$ and the assignment of diffraction planes are also provided as reference.

The PDF patterns of the three pre-catalyst samples are shown in Figure 3 with that of α-$MgCl_2$. The PDFs show the probability of the presence of atomic pairs with respect to the interatomic distance *r*. $G(r) = 0$ is the average, and a peak and a dip indicate a higher and lower density of atomic pairs, respectively. As shown in Figure 3a, α-$MgCl_2$ has clear peaks and dips down to $r = 10$ nm, indicating that an ordered structure exists over at least 10 nm. On the other hand, in ZNC-bm-DE, peaks and dips begin to decay from 2-4 nm, indicating that the long-range ordered structure is compromised. However, the peaks and dips do not completely flatten even at $r = 10$ nm, suggesting the existence of an ordered structure with a size of about 10 nm. On the other hand, in the two chemically prepared samples, decay occurs and proceeds dramatically from a shorter *r*. The signals become almost completely flat around $r = 4$ or 5 nm, which indicates that there is almost no long-range order above this distance. Comparing the PDFs of the three catalysts in the short-range region (Figure 3b), the positions of the major peaks and dips are similar for both the catalysts as for the α-$MgCl_2$, although there are differences in the *r*-dependent decay. This fact indicates that the crystal lattice of the Cl-Mg-Cl layer is virtually unaffected, even if the extent of activation is different.

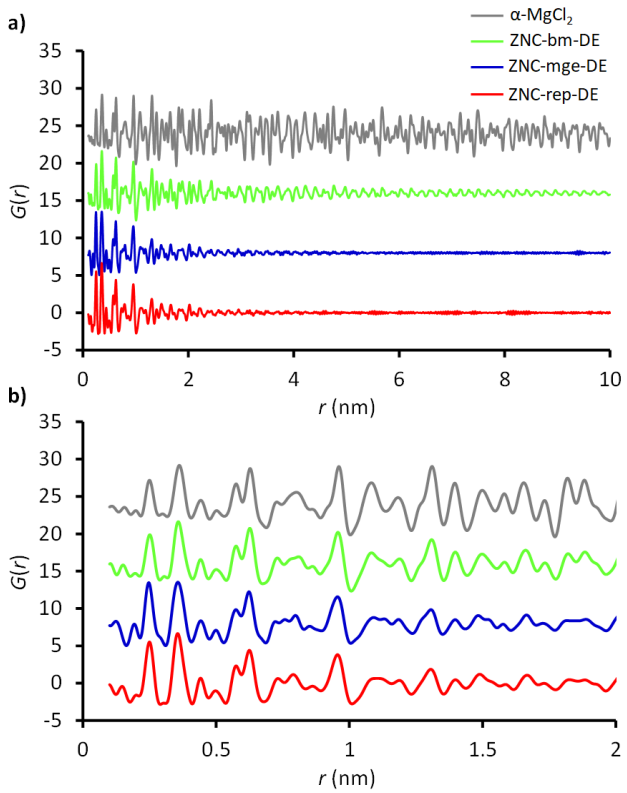

Figure 3. Part a) PDF patterns of ZNC-bm-DE (green), ZNC-mge-DE (blue), ZNC-rep-DE (red), and α-$MgCl_2$ for reference (gray). Part b) the magnified pattens up to r = 2 nm. All the patterns were vertically translated in for clarity.

In order to discuss the structural differences of the three pre-catalysts more quantitatively, XRD and PDF fitting were performed using $MgCl_2$ nanoparticle models. The details of nanoparticle model creation and fitting principle were reported previously [28]. Especially in PDF, the larger the r, the larger number of atomic pairs are involved in a peak, making the interpretation difficult, so fitting with molecular models is almost indispensable. The results of each XRD and PDF fitting are summarized in Figures S1-S4 and in Table S1, while the structural parameters are summarized in Table 2. In ZNC-bm-DE, $MgCl_2$ is present with crystallites of about 6 nm in the c direction, and 13 nm in the a,b directions, with Pc of about 49%. The decay observed in the PDF signal starting from 2-4 nm is likely attributed to the reduced crystallite size as well as to the stacking disorder among the Cl-Mg-Cl layers. The nanoparticle models determined for the two catalysts prepared by chemical routes were plate-like crystallites composed of only two Cl-Mg-Cl layers (L_c = ca. 1 nm). The lateral dimensions were about half to one-third the dimension of that of ZNC-dm-DE. It is interesting to observe that the difference in the lateral dimension of the $MgCl_2$ support qualitatively corresponds to the difference in the amount of Ti and DE. Indeed, smaller lateral dimension leads to a larger fraction of exposed Mg^{2+} cations available for stabilizing both adsorbates.

Table 2. $MgCl_2$ structural parameters determined by fitting the PXRD and PDF data of the three pre-catalysts, with different $MgCl_2$ nanoparticle models.

Catalyst	P_c (%)	L_c (nm)	$L_a \times L_b$ (nm)
ZNC-bm-DE	49	6.2	12.7 × 12.7
ZNC-mge-DE	25	0.9	5.5 × 3.3
ZNC-rep-DE	28	0.9	3.6 × 3.6

3.1.2. The 1,3-diether adsorption mode

IR spectroscopy was applied to elucidate the configuration of DE at the $MgCl_2$ surface in the three ZN pre-catalysts. Figure 4 shows the IR spectrum of pure DE (part a) compared to those of the three pre-catalysts and of the $MgCl_2$-DE sample (part b), the latter obtained by ball-milling together neat $MgCl_2$ and DE in the same conditions as in the synthesis of ZNC-bm-DE, but before adding $TiCl_4$. The IR spectrum of the pure compound (Figure 4a) is quite complex and is assigned with reference to those of similar ethers reported in the literature [30]. The group of bands in the 3000 – 2800 cm^{-1} is assigned to the stretching vibrational modes of CH_x species as follows: i) four bands are ascribed to the vibrational modes of the alkyl moieties, namely those at 2954 and 2870 cm^{-1} are due to $\nu_{asym}(CH_3)$ and to $\nu_{sym}(CH_3)$, while those at 2923 and 2834 cm^{-1} are due to the $\nu_{asym}(CH_2)$ and $\nu_{sym}(CH_2)$; ii) two bands at 2982 and 2889 cm^{-1} (the latter appearing as a shoulder of the more intense band at 2834 cm^{-1}) are assigned to the $\nu_{asym}(CH_3)$ and $\nu_{sym}(CH_3)$ modes of the methoxy groups; iii) finally, the sharp band at 2807 cm^{-1}, very low in position with respect to the common positions of $\nu(CH_x)$ in alkyl compounds, is assigned to $\nu(CH_2)$ of CH_2 moieties in agostic interaction with the oxygen of the ether group [31], either within the same molecule or from other molecules in the surrounding. The group of bands in the 1500 – 1300 cm^{-1} is assigned to the bending modes of the CH_x groups (1456 cm^{-1}, $\delta(CH_2)$, 1383 and 1366 cm^{-1}, $\delta(CH_3)$ of the isopropyl terminations). Finally, the intense band at 1100 cm^{-1} is diagnostic for the ν(C-O-C) vibration of the ether groups.

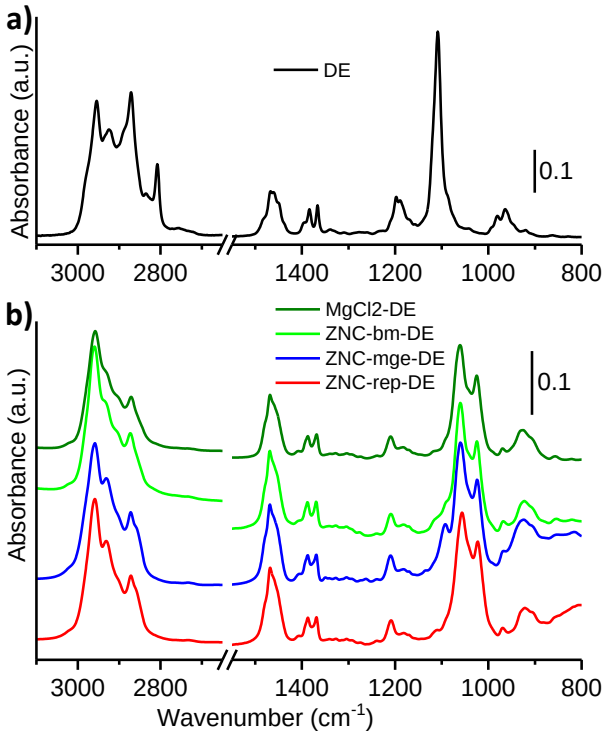

Figure 4. Part a) ATR-IR spectrum of neat DE. Part b) IR spectra of $MgCl_2$-DE (dark green), ZNC-bm-DE (green), ZNC-mge-DE (blue) and ZNC-rep-DE (red), all collected in transmission mode after diluting the samples in KBr. The spectra are vertically translated for clarity.

Similar IR bands can be recognized also in the spectrum of $MgCl_2$-DE (Figure 4b). There are two main evidences for DE interaction with $MgCl_2$ surface: i) the disappearance of the $\nu(CH_2)$ band at 2807 cm^{-1} that was ascribed to CH_2 groups in agostic interaction with the oxygen of the ether group; and ii) the downward shift and splitting of the ν(C-O-C) band into two components at 1060 and 1025 cm^{-1}. The first evidence suggests that, when DE is adsorbed on $MgCl_2$ surface, it loses the conformational freedom typical of the liquid phase. The shift of the ν(C-O-C) band at lower wavenumbers, instead, indicates that the ether group interacts with a Mg^{2+} cation at the $MgCl_2$ surface. The splitting of the ν(C-O-C) band is less straightforward, but it was already observed in the past for the polymeric $[MgCl_2(diether)]_n$ organometallic complex [32]. In that case all the diether molecules assumed the most stable chelated configuration [20, 33, 34] and the splitting of the band was explained in terms of non-equivalence of the chemical environment at each adsorption site [32].

The IR features of DE adsorbed on $MgCl_2$ can be clearly identified also in the spectra of the three pre-catalysts, with no additional bands that can suggest a direct interaction between DE and $TiCl_4$. As a matter of fact, ν(C-O-C) for a $TiCl_4$-diether complex was reported in literature by Cui *et al.* at 1020 and 997 cm^{-1} [35]. This result is in agreement with the co-adsorption model reported in the literature, which describes the adsorption process of donors as a competitive phenomenon with $TiCl_4$, where both species adsorb at the same unsaturated sites on different faces of $MgCl_2$ [21, 36-41], in close proximity but not in direct interaction. Unfortunately, DE signals are the same in the three pre-catalysts and do not allow to discriminate among the

different structural and morphological properties of $MgCl_2$ particles. Only in the spectrum of ZNC-mge-DE there is an additional band at 1092 cm^{-1}, which can be indicative of a family of slightly perturbed DE molecules (maybe trapped inside the pores) or which can be more reasonably due to the ν(C-O) of residual ethoxy species from the synthesis [27].

3.1.3. Electronic properties

The fact that the different synthetic procedures lead to different catalytic materials is indubitable just by looking at the powders appearance, ranging from bright yellow color in the case of ZNC-bm-DE to beige in the case of ZNC-rep-DE. The different colour indicates different electronic properties of the three pre-catalysts, which have been studied by DR UV-Vis spectroscopy. The spectra of the three pre-catalysts are shown in Figure 5.

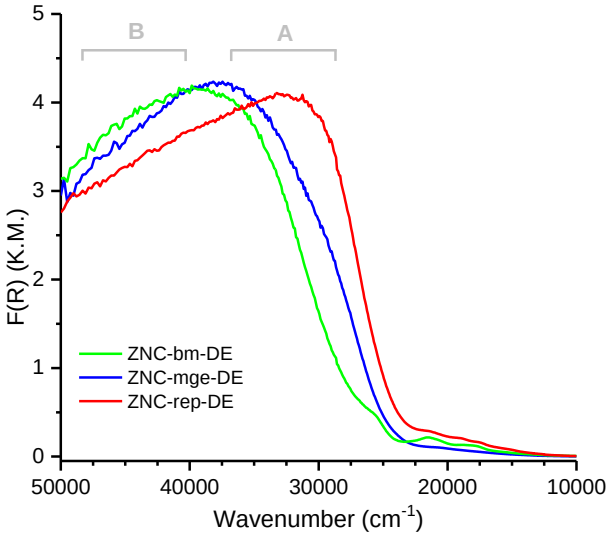

Figure 5. DR UV-Vis spectra of ZNC-bm-DE (green), ZNC-mge-DE (blue) and ZNC-rep-DE (red). The position of bands of type A and B was determined as the maximum of the second derivative curves, not shown for simplicity.

All spectra are characterized by a very intense absorption above 30000 cm^{-1}, with clear differences in position and shape, which are due to electronic transitions from the filled π orbitals of the Cl ligands to the vacant d orbitals of the Ti sites that, in the pre-catalysts, are supposed to be Ti^{4+} and hence to possess a d^0 electronic configuration. As recently discussed by some of us [42], octahedral coordination is assumed for the majority of Ti atoms, so that the Ti d orbitals are split into d_{t2g} and d_{eg} levels (separated in energy by the crystal-field splitting $\Delta_{CF} = 10\Delta q$). This causes a splitting of the charge-transfer absorption into two main bands [43], named A (corresponding to Cl(π) → Ti(d_{t2g})) and B (corresponding to Cl(π) → Ti(d_{eg})) in Figure 5. Moreover, because of the non-equivalence in energy of the orbitals of the different Cl ligands around the Ti centres, each transition is further split into several components, whose exact position was determined as the maximum of the second derivative curves. Figure 5 displays marked differences in the spectra of the three

pre-catalysts, despite the fact that the average Ti oxidation state and coordination geometry are expected to be the same.

In particular, the position of the band A is the most affected by the synthetic route (ZNC-rep-DE presents the band at the lowest energy, followed by ZNC-mge-DE, and finally by ZNC-bm-DE), whereas the position of the band B is more similar in all the cases. Following the same analysis of the electronic signals already reported in the literature [42], the crystal field-splitting Δ_{CF} value was obtained from the difference in energy between transitions B and A. ZNC-bm-DE shows the smallest Δ_{CF} equal to 11200 cm^{-1} (i.e., 1.39 eV), while ZNC-mge-DE and ZNC-rep-DE have much larger Δ_{CF}, almost similar to each other, respectively of 11950 and 12000 cm^{-1} (i.e., 1.48 and 1.49 eV). As a matter of comparison, Δ_{CF} = 1.43 eV was previously reported for a chemically activated ZN pre-catalyst similar to ZNC-mge-DE but containing dibutyl phthalate as internal donor, while much smaller Δ_{CF} values were found for a model $MgCl_2/TiCl_4$ sample obtained upon adsorption of $TiCl_4$ on bare high-surface-area $MgCl_2$ (Δ_{CF} = 0.99 eV) [42]. Δ_{CF} depends both on the nature of the ligands and on the effective oxidation state of Ti. Assuming a very similar nature of the Cl ligands in all the three pre-catalysts, the difference in the estimated Δ_{CF} indicates that the effective positive charge on the Ti sites is slightly different between the ZNC-bm-DE pre-catalyst and the industrial-like ones, ZNC-rep-DE and ZNC-mge-DE. The higher is Δ_{CF} value, the higher is the effective positive charge on the Ti centres. Correspondingly, a more positive Ti centre implies an easier charge transfer from the Cl ligands, as clearly indicated by the lower energy position of the A bands in ZNC-rep-DE and ZNC-mge-DE with respect to ZNC-bm-DE.

It is worth mentioning that the effective charge state of the Ti^{4+} sites in ZNC pre-catalysts is relevant for catalysis, because it has been demonstrated to inversely correlate with the activation energy for olefin insertion into the Ti-alkyl bond formed after activation: higher the Ti effective charge, easier the insertion of the olefin monomer [44]. Combining this result with the structural information obtained in Section 3.1.1 (in particular with the data reported in Table 2), we can reasonably conclude that smaller $MgCl_2$ crystallites reduce the transfer of electron density from $MgCl_2$ surface to $TiCl_4$ species, thus Ti^{4+} sites are more positively charged and, in turn, their intrinsic activity increases.

Curiously, beside the intense charge-transfer bands discussed above, all the spectra of the pre-catalysts shown in Figure 3 display a weak and broad absorption below 24000 cm^{-1}, more structured for ZNC-bm-DE than for the other two chemically prepared pre-catalysts. The origin of these signals is still uncertain, but the energy position suggests its assignment as d-d transitions of a minority of Ti^{3+} sites, present in the pre-catalysts already before the activation possibly because of side reaction of $TiCl_4$ during the synthesis. Anyhow, they do not seem to be involved in the following steps of the catalytic process (vide infra).

3.2. Spectroscopic investigation of TEAl-activated ZN catalysts

3.2.1. Electronic properties

All the three pre-catalysts were activated by TEAl, added in stoichiometric amount in hexane solution. Upon activation, the samples displayed a remarkable change of colour toward dark brown, thus suggesting a change in the Ti electronic properties. Figure 6 shows the DR UV-Vis spectra of the three catalysts before and after TEAl-activation in different amounts. In all the cases, the intense bands assigned to Cl(π) $\rightarrow$ Ti(d) charge-transfer transitions that dominate the spectra of the pre-catalysts (black curves) shift to higher wavenumbers after activation by TEAl (green, blue and red, respectively). This shift is indicative of the reduction of the 6-fold coordinated Ti^{4+} sites to Ti^{3+} [45]. Even though a quantitative evaluation is not possible, the almost complete disappearance of the original bands observed in the spectra of the pre-catalysts indicates that almost all Ti^{4+} sites have been reduced to Ti^{3+} by TEAl at an Al:Ti ratio of 2:1; when an intermediate ratio of 1:1 is adopted (grey curves), a weak shoulder at lower wavenumbers witnesses a minor fraction of residual unreduced Ti^{4+} sites.

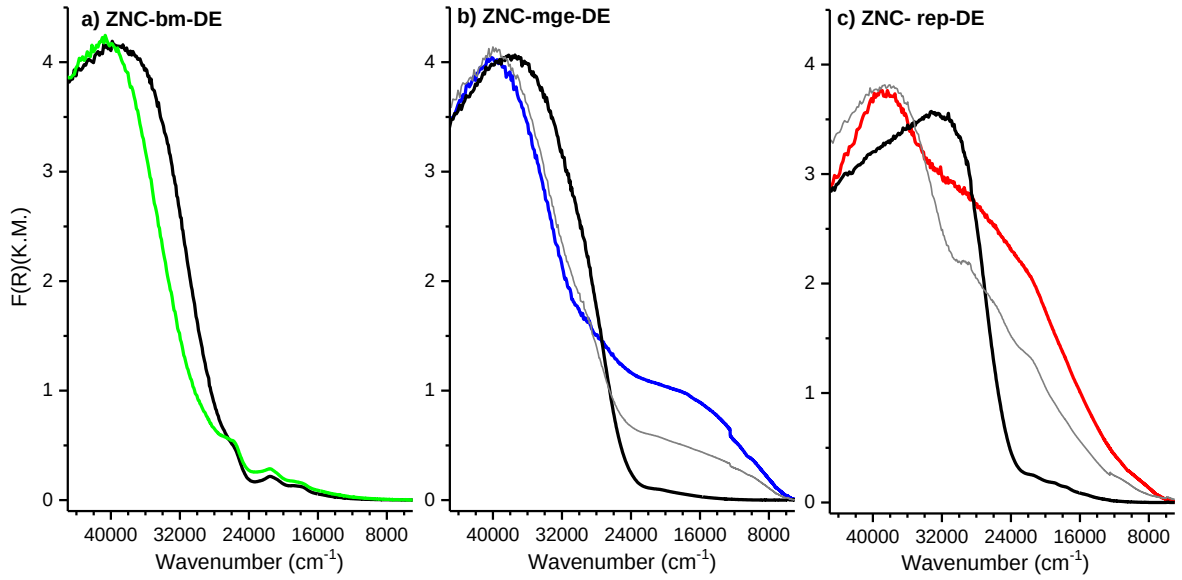

Figure 6. DR UV-Vis spectra of the three ZN catalysts activated by TEAl: black spectra are the spectra of the pre-catalysts already shown in Figure 5, green, blue and red spectra are those of the activated catalysts (Al:Ti=2:1), the grey spectra represent an intermediate step in the activation (Al:Ti=1:1) when present.

At the same time, new absorptions appear at lower wavenumbers. In the case of ZNC-bm-DE a very weak band is centred at ca. 22000 cm^{-1} (overlapped to the structured spectral features already present in the pre-catalyst, evidently not affected by TEAl), which can be assigned to Ti(d_{t2g}) $\rightarrow$ Ti(d_{eg}) d-d transition of an octahedral Ti^{3+} site with at least an alkyl group as a ligand (together with the pre-existing Cl^- ones) [46]. On the other hand, in the spectra of activated ZNC-rep-DE and ZNC-mge-DE an intense and broad band covers the entire spectral range from 24000 to 10000 cm^{-1}. Similar absorptions have already been reported in the literature for $TiCl_3$ salts and assigned to inter-site d-d transitions between neighbouring Ti^{3+} ions ($3d^1+3d^1\rightarrow$

$3d^0$+$3d^2$) connected to each other by a Cl^- bridge, where the electron movement through the bridge confers the partial charge transfer character to the electronic transition [47, 48]. Recently, the same features have been observed also in other TEAl-activated ZN catalysts and explained as due to the aggregation of $TiCl_3$-like clusters promoted by the severe reducing conditions caused by a high local concentration of TEAl molecules inside the accessible pores of the support material [42, 49]. This hypothesis is supported by the fact that the intensity of those signals in Figure 6b and c are strongly affected by the amount of TEAl used in the activation: for both ZNC-rep-DE and ZNC-mge-DE, when half of the TEAl is used for the activation (Al:Ti=1:1, grey spectra), the intensity of the band attributed to $TiCl_3$-like clusters is approximately the half. The phenomenon is more pronounced for ZNC-rep-DE than for ZNC-mge-DE, suggesting a higher Ti mobility and/or higher disorder and nanostructuration of the particles in the former.

It is important to remark that also in ZNC-mge-DE and ZNC-rep-DE catalysts most of the titanium is reasonably in the form of isolated Ti^{3+} sites, but their UV-Vis features are completely overshadowed by the more intense signals of the $TiCl_3$-like clusters, irrespectively to their amount.

3.2.2. Accessibility of the reduced Ti sites

In order to assess the amount of accessible Ti^{3+} sites in the three activated catalysts, CO adsorption at room temperature was monitored by IR spectroscopy as a function of time [50]. The evolution of the IR spectra along 60 minutes of experiment in the presence of CO (P_{CO}=200 mbar) are reported in Figure 7. In all the cases, the ν(C≡O) region is dominated by the roto-vibrational profile of CO gas (centred at 2143 cm^{-1}). However, weak bands are observed overlapped to this profile since the beginning of the experiment. Those above 2143 cm^{-1} are associated to CO weakly interacting with a few under-coordinated Mg^{2+} cations at the surface of $MgCl_2$ surface, ranging from 2194 to 2162 cm^{-1} depending on the acidic strength of Mg^{2+} adsorption sites [51, 52]. Those below 2143 cm^{-1}, instead, are ascribed to CO in interaction with Ti^{3+} sites [50, 53]. While on ZNC-bm-DE (Figure 7a) there are no bands in this region, in the cases of ZNC-mge-DE (Figure 7b) a band is observed at 2049 cm^{-1}, and for ZNC-rep-DE (Figure 7c) at 2056 cm^{-1}, both slowly growing in intensity over time. It is worth noticing that the position of the band is the balance between the polarizing effect of Ti^{3+} as a Lewis acid and the π-backdonation of the available $3d^1$ electron of the reduced titanium. Hence, the higher frequency of the band in ZNC-rep-DE reveals a higher positive charge on the Ti sites (in agreement with the analysis of the DR UV-Vis spectra of the pre-catalysts, Figure 5) which, in turn, should lead to a higher efficiency in olefin complexation and insertion through the agostic-assisted Cossee–Arlman mechanism [54].

At the same time, in both cases new bands appear and progressively grow up in the 1700-1550 cm^{-1} range, which is the typical spectral region of ν(C=O) for Ti-acyl species [50]. Ti-acyl species derive from CO insertion into the Ti^{3+}-ethyl bond [55, 56], with the position of ν(C=O) band that depends on the extent of the hapticity (η^2-coordination) of the acyl group with the Ti sites: a higher coordination weakens more the C=O

bond, shifting the v(C=O) band at lower wavenumbers. In the case of ZNC-mge-DE, only one v(C=O) band is observed at 1640 cm^{-1}, while in the case of ZNC-rep-DE there are two contributions at 1640 and 1595 cm^{-1}, indicative of at least two families of Ti species with a slightly different local structures, resulting in a different geometry for CO insertion. We speculate that this might be at the origin of the bimodal distribution in terms of lower and higher isotacticity typically observed in chemically prepared Ziegler-Natta catalysts, differently from the monomodal (lower isotactic) distribution obtained by mechanically prepared ones [57].

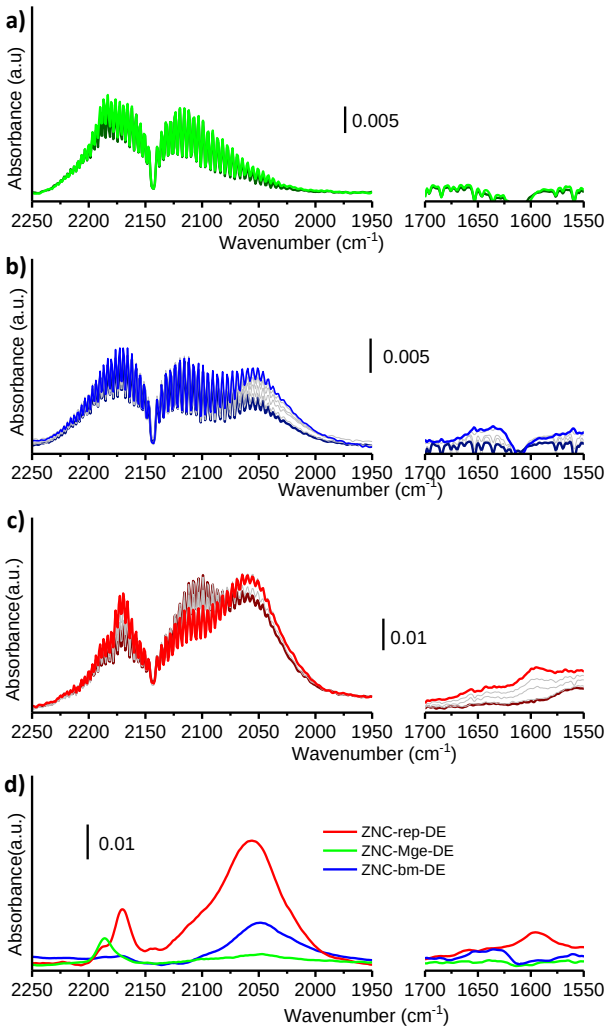

Figure 7. IR spectra of CO adsorbed at room temperature on activated ZNC-bm-DE (a), ZNC-mge-DE (b) and ZNC-rep-DE (c). In all the sequences, black spectra were collected just after CO dosage, while green, red and blue spectra after 60 minutes of interaction with CO; grey spectra were collected in between to show the evolution. Part d) Comparison of the three spectra collected after 60 minutes of interaction with CO, after normalizing the intensities to the optical thickness of the samples and subtracting the roto-vibrational features of CO gas.

In order to better compare the results obtained on the three catalysts and to extract quantitative information, the final spectra of each sequence (collected after 60 minutes of CO adsorption) have been normalized to the optical thickness of the sample pellets and shown in Figure 7d after subtracting the roto-

vibrational profile of CO gas. After data treatment, also in the case of ZNC-bm-DE a very weak signal of CO in interaction with Ti^{3+} can be identified at 2047 cm^{-1}. For ZNC-rep-DE the integrated area of the band assigned to CO adsorbed on Ti^{3+} is approximately 3.5 times greater than for ZNC-mge-DE, and roughly 20 times greater than for ZNC-bm-DE: these numbers give a roughly estimation of the relative amount of accessible Ti^{3+} sites in the three activated catalysts.

Altogether, DR UV-Vis and IR spectroscopic results prove that the pre-catalyst preparation route determines both the molecular structure of the active sites and their distribution, in agreement with previous studies based on the analysis of the produced polymers [57].

3.3. The catalysts in action: kinetics of propylene polymerization

The reaction rate of propylene polymerization in the presence of the three activated catalysts was assessed by monitoring the gas consumption over time in static conditions: a quartz reactor tube containing the powder of the TEAl-activated catalyst was fed with 200 mbar of propylene at room temperature, continuously recording the dropping pressure during the reaction process. Figure S5 shows, for the sake of example, propylene pressure as a function of time during the polymerization in the presence of TEAl-activated ZNC-rep-DE. The gas pressure decreases with a parabolic trend, rapidly dropping down at the beginning of the reaction, then slowly reaching a plateau when most of the propylene was consumed. The reaction order was evaluated, looking for a linear correlation over time of either the natural logarithm of the pressure (in the assumption of a first-order reaction) or of the reciprocal of pressure (in the assumption of a second-order reaction). Accordingly, the second-order resulted to be the model that better describes the evolution of the process (as clearly displayed in Figure S6). This is compatible with the so-called “monomer-triggered insertion mechanism”, where the migration of the alkyl group onto the coordinated molecule of monomer is favoured by the presence of another molecule simultaneously taking its place [58].

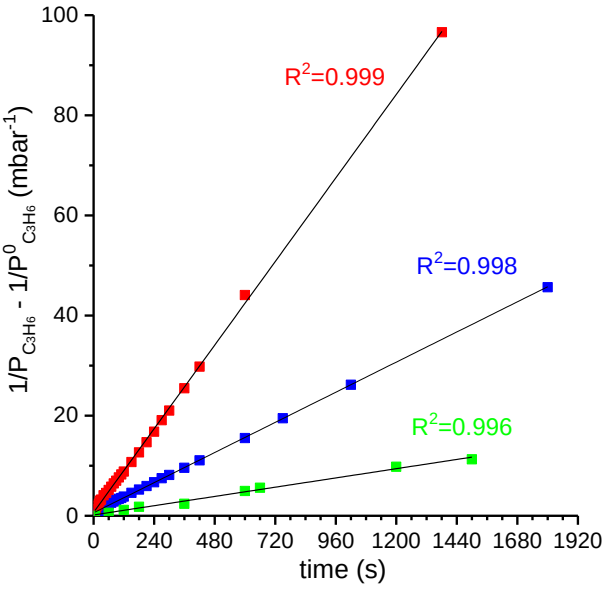

Figure 8. Kinetics of propylene polymerization on the three catalysts activated by TEAl with an Al:Ti ratio of 2:1. The experimental data (dots) are plotted in terms of reciprocal of monomer pressure (after subtraction of the initial pressure reciprocal) as a function of time and fitted according to second order kinetic law (lines). The goodness of the fit is also reported.

By applying the second-order model to all the catalysts it is possible to compare their activity. Figure 8 displays the kinetics of propylene polymerization for the catalysts activated by TEAl with an Al:Ti ratio of 2:1. After normalizing the kinetics per the amount of Ti, the rate constants for ZNC-rep-DE, ZNC-mge-DE and ZNC-bm-DE are 0.07, 0.02 and 0.007 $s^{-1}\,mbar^{-1}\,mol_{Ti}^{-1}$, respectively. It is interesting to note that this trend recalls the trend in the ability to coordinate CO (Figure 7d). Both the accessibility and the intrinsic nature of the active sites contribute to the different polymerization kinetics. Since there is no supply of fresh TEAl during polymerization in the gas phase experiment shown in Figure 8, the result cannot be used to discuss the intrinsic nature of the active sites, but it is indicative for the amount of accessible Ti species formed by TEAl before the contact with the monomer. In this sense, it is possible to correlate the different catalytic performances with the adopted catalyst preparation methods.

Curiously, when the three Ziegler-Natta catalysts were activated by a lower amount of TEAl (Al:Ti=1:1), the kinetics of propylene polymerization was drastically slower (as shown in Figure S7), with no significant differences between ZNC-rep-DE and ZNC-mge-DE (both of them presenting a rate constant of 0.02 $s^{-1}\,mbar^{-1}\,mol_{Ti}^{-1}$) and almost no activity by ZNC-bm-DE. Evidently, the process requires at least an Al:Ti ratio of 2:1 to guarantee the proper activation of the catalysts (as observed also by DR UV-Vis spectroscopy in Figure 6) and to scavenge adventitious contaminations within the reactor during the polymerization.

4. Conclusions

In this work, three different ZN catalysts belonging to the 5th generation were deeply investigated in terms of particles morphology, surface species, electronic properties of the Ti sites, and catalytic activity. The multi-technique approach adopted herein allowed the full characterization of three the catalysts at each step of their life, from the synthesis (pre-catalysts) to the activation by TEAl (activated catalysts) and their employment in propylene polymerization (catalysts in action).

Irrespective of the synthetic route, the 1,3-diether internal donor (DE) exclusively interacts with the $MgCl_2$ surface, and no evidence for a direct interaction with the Ti sites was found. This substantiates the co-adsorption model reported in the literature, which describes the adsorption process of the internal electron donors as a competitive phenomenon with $TiCl_4$, both species adsorbing at the same unsaturated sites on $MgCl_2$ surface. On the other hand, the synthetic routes determine different structure and size for $MgCl_2$ particles, the reprecipitation chemical method bringing to the smallest $MgCl_2$ nanoparticles. This in turn influences the electronic properties of the Ti sites and their local structure. In particular, according to DR UV-Vis spectroscopy, the chemically synthetized pre-catalysts present a higher effective positive charge on the Ti sites with respect to ZNC-bm-DE.

Upon TEAl-activation, alkylated Ti^{3+} species are formed, which are detectable either by UV-Vis spectroscopy or by IR spectroscopy of adsorbed CO, or both. In the case of the chemically prepared catalysts also inactive $TiCl_3$-like clusters are formed, likely because of TEAl over-concentration in correspondence of intra-particles pores. Indeed, they are formed in larger amount at higher TEAl amount and on the ZNC-rep-DE catalyst, which is that characterized by the smallest $MgCl_2$ particles. The accessibility of the Ti^{3+} sites was assessed by IR spectroscopy of CO adsorbed at room temperature: ZNC-rep-DE has approximately 3.5 times more accessible Ti^{3+} sites than ZNC-mge-DE, and almost 20 times more than ZNC-bm-DE. Furthermore, especially in the case of ZNC-rep-DE, CO adsorption revealed the presence of two main families of activated Ti sites with slightly different geometries for CO insertion, which can tentatively be interpreted as responsible for two different fractions of lower and higher isotactic polypropylene typically produced by chemically prepared ZN catalysts.

The three activated catalysts display substantially different kinetics of propylene polymerization in very mild conditions. The kinetic data correlate well with the amount of accessible Ti^{3+} sites as determined by IR spectroscopy of adsorbed CO, but also with the effective positive charge on the Ti^{4+} sites in the pre-catalysts as determined by UV-Vis spectroscopy. This demonstrates the potential of spectroscopic methods in providing information useful to understand and/or predict the catalytic performance of ZN catalysts.
This information will serve as guidelines for the preparation and use of 5th generation Ziegler-Natta catalysts depending on the targeted properties and, in turn, final application.

REFERENCES

[1] P. Galli, G. Vecellio, Technology: driving force behind innovation and growth of polyolefins, Prog. Polym. Sci., 26 (2001) 1287-1336.
[2] V. Busico, Metal-catalysed olefin polymerisation into the new millennium: a perspective outlook, Dalton Trans., (2009) 8794-8802.
[3] E. Groppo, K. Seenivasan, C. Barzan, The potential of spectroscopic methods applied to heterogeneous catalysts for olefin polymerization, Catal. Sci. Technol., 3 (2013) 858-878.
[4] A. Piovano, E. Groppo, Flexible ligands in heterogeneous catalysts for olefin polymerization: Insights from spectroscopy, Coord. Chem. Rev., 451 (2022) 214258.
[5] J.C.J. Bart, Activation of magnesium chloride by dry milling, J. Mater. Sci., 28 (1993) 278-284.
[6] F. Delogu, G. Mulas, L. Schiffini, G. Cocco, Mechanical work and conversion degree in mechanically induced processes, Mater. Sci. Eng., A, 382 (2004) 280-287.
[7] L. Brambilla, G. Zerbi, F. Piemontesi, S. Nascetti, G. Morini, Structure of MgCl2-TiCl4 complex in co-milled Ziegler-Natta catalyst precursors with different TiCl4 content: Experimental and theoretical vibrational spectra, J. Mol. Catal. A-Chem., 263 (2007) 103-111.
[8] A. Dashti, A. Ramazani Sa, Y. Hiraoka, S.Y. Kim, T. Taniike, M. Terano, Kinetic and morphological study of a magnesium ethoxide-based Zieglerâ€“Natta catalyst for propylene polymerization, Polym. Int., 58 (2009) 40-45.
[9] D.H. Lee, Y.T. Jeong, K. Soga, In situ formation of magnesium chloride support and internal donor during preparation of propylene polymerization catalysts, Ind. Eng. Chem. Res., 31 (1992) 2642-2647.
[10] T. Funako, P. Chammingkwan, T. Taniike, M. Terano, Alternation of Pore Architecture of Ziegler-Natta Catalysts through Modification of Magnesium Ethoxide, Macromol. React. Eng., 9 (2015) 325-332.
[11] J.S. Chung, I.K. Song, W.Y. Lee, H.M. Park, Morphology control of a MgCl2-supported Ziegler-Natta catalyst by the recrystallization method, Macromol. Chem. Phys., 196 (1995) 1205-1210.
[12] J.H. Choi, J.S. Chung, H.W. Shin, I.K. Song, W.Y. Lee, The effect of alcohol treatment in the preparation of MgCl2 support by a recrystallization method on the catalytic activity and isotactic index for propylene polymerization, Eur. Polym. J., 32 (1996) 405-410.
[13] A. Parada, T. Rajmankina, J. Chirinos, Study of the MgCl2 recrystallization conditions on Ziegler-Natta catalyst properties, Polym. Bull., 43 (1999) 231-238.
[14] P. Piyavit, P. Piyasan, Comparison of Activity of Ziegler-Natta Catalysts Prepared by Recrystallization and Chemical Reaction Methods towards Polymerization of Ethylene, ENGINEERING JOURNAL, 13 (2009) 57-64.
[15] A.K. Yaluma, P.J.T. Tait, J.C. Chadwick, Active center determinations on MgCl2-supported fourth- and fifth-generation Ziegler–Natta catalysts for propylene polymerization, J. Polym. Sci. A Polym. Chem., 44 (2006) 1635-1647.
[16] G.D. Bukatov, D.K. Maslov, S.A. Sergeev, M.A. Matsko, Effect of internal donors on the performance of Ti-Mg catalysts in propylene polymerization: Donor introduction during or after MgCl2 formation, Appl. Catal. A: Gen., 577 (2019) 69-75.
[17] B.R. Paghadar, J.B. Sainani, S.K. M, P. Bhagavath, Internal donors on supported Ziegler Natta catalysts for isotactic polypropylene: a brief tutorial review, J. Polym. Res., 28 (2021) 402.
[18] M. Nikolaeva, M. Matsko, V. Zakharov, Propylene polymerization over supported Ziegler–Natta catalysts: Effect of internal and external donors on distribution of active sites according to stereospecificity, J. Appl. Polym. Sci., 135 (2018) 46291.
[19] A.G. Potapov, L.V. Politanskaya, The study of the adsorption of 1,3-diethers on the MgCl2 surface, J. Mol. Catal. A Chem., 368-369 (2013) 159-162.
[20] R. Credendino, D. Liguori, G. Morini, L. Cavallo, Investigating phthalate and 1,3-diether coverage and dynamics on the (104) and (110) surfaces of MgCl2-supported Ziegler-Natta catalysts, Journal of Physical Chemistry C, 118 (2014) 8050-8058.
[21] A. Correa, F. Piemontesi, G. Morini, L. Cavallo, Key Elements in the Structure and Function Relationship of the MgCl2/TiCl4/Lewis base Ziegler-Natta Catalytic System, Macromol., 40 (2007) 9181-9189.

[22] M. Ghashghaee, H. Arabi, M. Ghambarian, Molecular-level insights into adsorption of a novel silyl ester donor on essential MgCl2 facets of supported Ziegler–Natta catalysts, J. Phys. Chem. Solids, 159 (2021) 110249.
[23] G. Morini, E. Albizzati, G. Balbontin, I. Mingozzi, M.C. Sacchi, F. Forlini, I. Tritto, Microstructure Distribution of Polypropylenes Obtained in the Presence of Traditional Phthalate/Silane and Novel Diether Donors: A Tool for Understanding the Role of Electron Dnors in MgCl2-Supported Ziegler-Natta Catalysts. , Macromolecules, 29 (1996) 5770−5776.
[24] T. Wada, A. Thakur, P. Chammingkwan, M. Terano, T. Taniike, A. Piovano, E. Groppo, Structural Disorder of Mechanically Activated δ-MgCl2 Studied by Synchrotron X-ray Total Scattering and Vibrational Spectroscopy, Catalysts, 10 (2020) 1089.
[25] M. Terano, H. Soga, K. Kimura, Catalyst for Polymerization of Olefins, in, Toho Titanium Co., Ltd., 1989.
[26] M. Kioka, H. Kitani, N. Kashiwa, Process for producing olefin polymers or copolymers, in, Mitsui Petrochemical Industries, Ltd., 1982.
[27] A. Piovano, T. Wada, A. Amodio, G. Takasao, T. Ikeda, D. Zhu, M. Terano, P. Chammingkwan, E. Groppo, T. Taniike, Formation of Highly Active Ziegler–Natta Catalysts Clarified by a Multifaceted Characterization Approach, ACS Catal., 11 (2021) 13782-13796.
[28] T. Wada, G. Takasao, A. Piovano, M. D'Amore, A. Thakur, P. Chammingkwan, P.C. Bruzzese, M. Terano, B. Civalleri, S. Bordiga, E. Groppo, T. Taniike, Revisiting the identity of δ-MgCl2: Part I. Structural disorder studied by synchrotron X-ray total scattering, J. Catal., 385 (2020) 76-86.
[29] X. Qiu, J.W. Thompson, S.J.L. Billinge, PDFgetX2: a GUI-driven program to obtain the pair distribution function from X-ray powder diffraction data, J. Appl. Cryst., 37 (2004) 678-678.
[30] K. Kumar, A.L. Verma, Molecular conformation of 2,2-dimethoxypropane, J. Mol. Struct., 22 (1974) 173-181.
[31] E.-L. Zins, B. Silvi, M.E. Alikhani, Activation of C–H and B–H bonds through agostic bonding: an ELF/QTAIM insight, Phys. Chem. Chem. Phys., 17 (2015) 9258-9281.
[32] V.H. Nissinen, I.O. Koshevoy, T.T. Pakkanen, Crystalline magnesium chloride-electron donor complexes: new support materials for Ziegler-Natta catalysts, Dalton Trans., 46 (2017) 4452-4460.
[33] J.W. Lee, W.H. Jo, Chemical structure–stereospecificity relationship of internal donor in heterogeneous Ziegler–Natta catalyst for propylene polymerization by DFT and MM calculations, J. Organomet. Chem., 694 (2009) 3076-3083.
[34] L. Brambilla, G. Zerbi, F. Piemontesi, S. Nascetti, G. Morini, Structure of Donor Molecule 9,9-Bis(Methoxymethyl)-Fluorene in Ziegler-Natta Catalyst by Infrared Spectroscopy and Quantum Chemical Calculation, Journal of Physical Chemistry C, 114 (2010) 11475-11484.
[35] N. Cui, Y. Ke, H. Li, Z. Zhang, C. Guo, Z. Lv, Y. Hu, Effect of diether as internal donor on MgCl2-supported Ziegler–Natta catalyst for propylene polymerization, J. Appl. Polym. Sci., 99 (2006) 1399-1404.
[36] T. Taniike, M. Terano, Coadsorption and support-mediated interaction of ti species with ethyl benzoate in MgCl2-Supported heterogeneous ziegler-natta catalysts studied by density functional calculations, Macromol. Rapid Commun., 28 (2007) 1918-1922.
[37] T. Taniike, M. Terano, Coadsorption model for first-principle description of roles of donors in heterogeneous Ziegler-Natta propylene polymerization, J. Catal., 293 (2012) 39-50.
[38] D.V. Stukalov, V.A. Zakharov, I.L. Zilberberg, Adsorption species of ethyl benzoate in MgCl2-supported ziegler-natta catalysts. A density functional theory study, Journal of Physical Chemistry C, 114 (2010) 429-435.
[39] A.S. Bazhenov, P. Denifl, T. Leinonen, A. Pakkanen, M. Linnolahti, T.A. Pakkanen, Modeling Coadsorption of Titanium Tetrachloride and Bidentate Electron Donors on Magnesium Dichloride Support Surfaces, Journal of Physical Chemistry C, 118 (2014) 27878-27883.
[40] A. Vittoria, A. Meppelder, N. Friederichs, V. Busico, R. Cipullo, Demystifying Ziegler-Natta Catalysts: The Origin of Stereoselectivity, ACS Catal., 7 (2017) 4509-4518.
[41] X. Guo, L. Cui, Y. Wang, J. Yi, J. Sun, Z. Liu, B. Liu, Mechanistic Study on Effect of Electron Donors in Propylene Polymerization Using the Ziegler–Natta Catalyst, Journal of Physical Chemistry C, 125 (2021) 8533-8542.

[42] A. Piovano, M. Signorile, L. Braglia, P. Torelli, A. Martini, T. Wada, G. Takasao, T. Taniike, E. Groppo, Electronic Properties of Ti Sites in Ziegler–Natta Catalysts, ACS Catal., 11 (2021) 9949-9961.
[43] B.N. Figgis, Introduction to ligand fields, John Wiley & Sons, New York, 1966.
[44] G. Takasao, T. Wada, A. Thakur, P. Chammingkwan, M. Terano, T. Taniike, Insight into structural distribution of heterogeneous Ziegler–Natta catalyst from non-empirical structure determination, J. Catal., 394 (2021) 299-306.
[45] C.K. Jorgensen, Electron Transfer Spectra, Progr. Inorg. Chem. , 12 (1970) 101-157.
[46] P. Atkins, T. Overton, J. Rourke, M. Weller, F. Armstrong, Shriver and Atkins' Inorganic Chemistry, 5th ed., Oxford University Press, New York, 2010.
[47] R.J.H. Clark, Diffuse Reflectance Spectra of Some Anhydrous Transition-Metal Halides., J. Chem. Soc., 0 (1964) 417-425.
[48] G. Baldini, I. Pollini, G. Spinolo, Optical Properties of α- and β-TiCl3, Phys. Stat. Sol., 27 (1968) 95-100.
[49] A. Piovano, E. Morra, M. Chiesa, E. Groppo, Tuning the Ti3+ and Al3+ Synergy in an Al2O3/TiClx Catalyst to Modulate the Grade of the Produced Polyethylene, ACS Catal., 7 (2017) 4915-4921.
[50] A. Piovano, J. Zarupski, E. Groppo, Disclosing the Interaction between Carbon Monoxide and Alkylated Ti3+ Species: a Direct Insight into Ziegler–Natta Catalysis, J. Phys. Chem. Lett., 11 (2020) 5632-5637.
[51] V.A. Zakharov, E.A. Paukshtis, T.B. Mikenas, A.M. Volodin, E.N. Vitus, A.G. Potapov, Surface acidic sites of highly disperse magnesium chloride: IR and ESR spectroscopy studies, Macromol. Symp., 89 (1995) 55-61.
[52] M. D'Amore, K.S. Thushara, A. Piovano, M. Causà, S. Bordiga, E. Groppo, Surface Investigation and Morphological Analysis of Structurally Disordered MgCl2 and MgCl2/TiCl4 Ziegler–Natta Catalysts, ACS Catal., 6 (2016) 5786–5796.
[53] P. Pletcher, A. Welle, A. Vantomme, B.M. Weckhuysen, Quality control for Ziegler-Natta catalysis via spectroscopic fingerprinting, J. Catal., 363 (2018) 128-135.
[54] P. Cossee, Ziegler-Natta catalysis I. Mechanism of polymerization of α-olefins with Ziegler-Natta catalysts, J. Catal., 3 (1964) 80-88.
[55] M. Bochmann, L.M. Wilson, M.B. Hursthouse, R.L. Short, Cationic alkylbis(cyclopentadienyl)titanium complexes. Synthesis, reactions with carbon monoxide and tert-butyl isocyanide, and the structure of [Cp2Ti[.eta.2-C(Me)NBu-tert](CNBu-tert)]BPh4.MeCN, Organometallics, 6 (1987) 2556-2563.
[56] F. Calderazzo, Synthetic and Mechanistic Aspects of Inorganic Insertion Reactions. Insertion of Carbon Monoxide, Angew. Chem. Int. Ed. Engl., 16 (1977) 299-311.
[57] Y. Hiraoka, S.Y. Kim, A. Dashti, T. Taniike, M. Terano, Similarities and Differences of the Active Sites in Basic and Advanced MgCl2-Supported Ziegler-Natta Propylene Polymerization Catalysts, Macromol. React. Eng., 4 (2010) 510-515.
[58] M. Ystenes, The trigger mechanism for polymerization of alpha-olefins with Ziegler-Natta catalysts - a new model based on interaction of 2 monomers at the transition-state and monomer activation of the catalytic centers, J. Catal., 129 (1991) 383-401.